Imaging robust microglial activation after lipopolysaccharide administration in humans with PET

Christine M. Sandiego[a,b], Jean-Dominique Gallezot[b], Brian Pittman[a], Nabeel Nabulsi[b], Keunpoong Lim[b], Shu-Fei Lin[b], David Matuskey[a,b], Jae-Yun Lee[c], Kevin C. O'Connor[c], Yiyun Huang[b], Richard E. Carson[b], Jonas Hannestad[d], and Kelly P. Cosgrove[a,b,1]

[a]Department of Psychiatry, Yale University, New Haven, CT 06511; [b]PET Center, Diagnostic Radiology, Yale University, New Haven, CT 06520; [c]Department of Neurology, Yale University, New Haven, CT 06511; and [d]UCB Pharma, Braine-l'Alleud, Belgium

Edited by Joanna S. Fowler, Brookhaven National Laboratory, Upton, NY, and approved August 4, 2015 (received for review June 4, 2015)

Neuroinflammation is associated with a broad spectrum of neurodegenerative and psychiatric diseases. The core process in neuroinflammation is activation of microglia, the innate immune cells of the brain. We measured the neuroinflammatory response produced by a systemic administration of the *Escherichia coli* lipopolysaccharide (LPS; also called endotoxin) in humans with the positron emission tomography (PET) radiotracer [^{11}C]PBR28, which binds to translocator protein, a molecular marker that is up-regulated by microglial activation. In addition, inflammatory cytokines in serum and sickness behavior profiles were measured before and after LPS administration to relate brain microglial activation with systemic inflammation and behavior. Eight healthy male subjects each had two 120-min [^{11}C]PBR28 PET scans in 1 d, before and after an LPS challenge. LPS (1.0 ng/kg, i.v.) was administered 180 min before the second [^{11}C]PBR28 scan. LPS administration significantly increased [^{11}C]PBR28 binding 30–60%, demonstrating microglial activation throughout the brain. This increase was accompanied by an increase in blood levels of inflammatory cytokines, vital sign changes, and sickness symptoms, well-established consequences of LPS administration. To our knowledge, this is the first demonstration in humans that a systemic LPS challenge induces robust increases in microglial activation in the brain. This imaging paradigm to measure brain microglial activation with [^{11}C]PBR28 PET provides an approach to test new medications in humans for their putative antiinflammatory effects.

neuroinflammation | PBR28 | endotoxin | microglia | cytokines

The immune system plays a vital role in the response to infection and injury, and activation of the immune system in the context of central nervous system (CNS) diseases likely contributes to the pathophysiology of these diseases. Multiple sclerosis is the prototypical neuroinflammatory disease (1); however, a role for the immune system has been proposed in the pathogenesis of several other CNS diseases including Alzheimer's, Parkinson's, amyotrophic lateral sclerosis, epilepsy, depression, and addictive disorders (2–8). Loss of neurons or impairment of neuronal function underlying these diseases may be caused or exacerbated by neuroinflammation, which results from chronic activation of microglia, the primary immune surveillance cells of the brain. Microglia are ubiquitous in the CNS and are necessary for the removal of damaged cells and promotion of tissue repair (9–11). However, dysregulation in peripheral and central inflammatory cytokine signaling interrupts normal microglial function, leading to neuronal dysfunction, neurotoxicity, neurodegeneration, and attenuated neurogenesis (3, 5, 12), processes that underlie most CNS diseases and result in deleterious effects on behavior, mood, motivation, and possibly cognition (11, 13–15). Accumulating evidence for a role of immune dysregulation and neuroinflammation in CNS diseases has attracted the attention of the pharmaceutical industry, and several companies are active in the development of drugs targeting the immune response pathway. The ability to measure microglial activation in the human brain in vivo is an essential tool for the development and testing of new medications that regulate the inflammatory processes.

When microglia are activated from their resting state, they express high levels of the 18-kDa translocator protein (TSPO), which can be measured in vivo in the brain with the positron emission tomography (PET) radiotracer [^{11}C]PBR28 (16–19). TSPO is present on the outer mitochondrial membrane of microglia, and one established function of TSPO is to transport cholesterol to the inner mitochondrial membrane for the production of steroids, with possible additional functions in regulating cell death, cytokine production, and microglial proliferation (20). Recent studies have also found that TSPO itself has a role in regulating microglial immune function, as antagonists of TSPO reduce the activation of microglia (21). Significantly higher TSPO expression, measured with [^{11}C]PBR28 and PET, was recently found in cortical brain regions of patients with early onset Alzheimer's disease compared with subjects with mild cognitive impairment and healthy controls (22), which highlights the potential role of neuroinflammation in the etiology of Alzheimer's disease (6). However, studies examining TSPO expression between healthy control subjects and other patient groups such as multiple sclerosis, depression, or cocaine abusers (23–27) have produced mixed results. A well-established and robust preclinical model uses the administration of *Escherichia coli* lipopolysaccharide (LPS; also called endotoxin) to trigger "classic" activation of microglia and has been used in rodents to study neurodegeneration (28–31). We previously reported a significant increase in [^{11}C]PBR28 binding at 1 (29%) and 4 (62%) hours after LPS administration in nonhuman primates (NHPs) compared with baseline binding levels (32).

Significance

Neuroinflammation is a brain immune response that is associated with neurodegenerative diseases and is primarily driven by activation of microglia, the brain's resident macrophages. Dysfunctional microglial activation may contribute to the behavioral changes observed in neurodegenerative diseases. Upon activation, microglia express translocator protein, which can be imaged with the radiotracer [^{11}C]PBR28 and positron emission tomography (PET) in the living human brain. We imaged healthy human subjects with [^{11}C]PBR28 and PET before and after i.v. administration of lipopolysaccharide (LPS), a potent immune activator. LPS produced a marked increase in brain microglial activation, peripheral inflammatory cytokine levels, and self-reported sickness symptoms. This imaging paradigm can provide a direct approach to test new medications for their potential to reduce acute neuroinflammation.

Author contributions: J.H. and K.P.C. designed research; C.M.S., N.N., K.L., S.-F.L., D.M., J.-Y.L., K.C.O., Y.H., R.E.C., and K.P.C. performed research; C.M.S., J.-D.G., and B.P. analyzed data; D.M. is the medical doctor (M.D.) on study; K.C.O. provided immunology expertise; Y.H. senior radiochemist; R.E.C. checked analysis and helped with writing; and C.M.S. and K.P.C. wrote the paper.

The authors declare no conflict of interest.

This article is a PNAS Direct Submission.

[1]To whom correspondence should be addressed. Email: kelly.cosgrove@yale.edu.

www.pnas.org/cgi/doi/10.1073/pnas.1511003112

Moreover, such an increase in [^{11}C]PBR28 binding was associated with concurrent elevations in peripheral inflammatory cytokine levels and immunohistochemical evidence for neuroinflammation and TSPO expression in the brain.

In this study, we translated this innovative paradigm to humans to enable the measurement of LPS-induced increases in activated microglia in the brain of living human subjects. If proved successful, such a research paradigm could be a quantitative imaging biomarker of a neuroimmune response and thus incredibly useful to evaluate the effect of antiinflammatory medications in the human brain.

Results

All subjects (n = 8) participated in two 120-min [^{11}C]PBR28 PET scans on the same day. LPS (1 ng/kg, i.v. bolus) was administered 3 h before the second PET scan based on (*i*) the timing of the neuroinflammatory response observed in our previous nonhuman primate study (32) and (*ii*) the time course of the peripheral inflammatory response in humans (33). For each scan, [^{11}C]PBR28 was injected as a 1-min bolus (13.9 ± 1.1 mCi). There were no significant differences between baseline and post-LPS scan conditions in the following parameters: injected activity (15.9 ± 3.9 and 12.8 ± 4.9 mCi), injected mass (0.026 ± 0.036 and 0.024 ± 0.038 µg), and radiotracer plasma-free fraction (0.031 ± 0.006 and 0.031 ± 0.008).

LPS Significantly Increases [^{11}C]PBR28 Binding in the Human Brain. Due to an rs6971 polymorphism on the TSPO gene that affects binding of PBR28 and other TSPO tracers (34), all subjects were genotyped for TSPO binding status before the scans to exclude nonbinders of [^{11}C]PBR28. Accordingly, only high-affinity binding (HAB, n = 3) and mixed-affinity binding (MAB, n = 5) subjects were included. [^{11}C]PBR28 volume of distribution (V_T), which is proportional to the availability of TSPO binding sites, was measured in regions of interest for baseline and LPS challenge scans, and the change in V_T (%ΔV_T) was calculated and reported as mean ± SEM (Table 1). Baseline V_T values were two times higher in HAB compared with MAB subjects, consistent with results from other studies (34, 35). However, there was no significant difference in %ΔV_T between HAB (39 ± 12%, n = 3) and MAB (50 ± 10%, n = 5) subjects ($F_{1,6} = 0.70$, $P = 0.43$); therefore all subjects were combined for further analysis. In the model comparing %ΔV_T across regions, LPS administration significantly increased [^{11}C]PBR28 binding (V_T) by an average of 46 ± 8%, and the increase averaged across regions was observed in all subjects (Fig. 1). A significant main effect of region was observed ($F_{9,54} = 3.5$, $P < 0.0019$). Least-square means estimated from the model for %ΔV_T within each region were all significantly greater than zero. The mean % increase in [^{11}C]PBR28 binding (V_T) ranged from 31% in the thalamus to 63% in the parietal cortex.

Physiological Responses to LPS Administration. Vital signs were closely monitored after LPS administration. By the start of the LPS challenge scan, there was a nonclinically significant decrease in systolic (−5 mmHg) and diastolic (−10 mmHg) blood pressure, and an increase in heart rate (+25 bpm) and temperature (+2.0 °C) from baseline levels, consistent with findings from previous studies (32, 36).

LPS Increases Peripheral Inflammatory Cytokine Levels. Blood samples were collected (relative to LPS administration; t = 0 min) at −10 (baseline), 60, 90, 120, 180 (start of post-LPS [^{11}C]PBR28) and 240 min to measure serum levels of TNF-α, IL-6, IL-8, IL-10, and IFN-γ (Fig. 2*A*). LPS administration resulted in significantly increased levels of TNF-α (time effect: $F_{4,27} = 9.8$, $P < 0.001$), IL-6 ($F_{4,7} = 8.5$, $P = 0.008$), IL-8 ($F_{4,27} = 11.0$, $P < 0.001$), and IL-10 ($F_{4,7} = 13.7$, $P = 0.002$), with maximum increases occurring at 120–180 min (P = 0.001–0.0001), followed by gradual decreases. Increases of IFN-γ displayed no statistically significant differences across time points compared with baseline levels ($F_{4,7} = 2.6$, $P = 0.13$). In general, these findings are consistent with the well-established systemic response to LPS (33, 37).

Table 1. [^{11}C]PBR28 regional V_T values (mean ± SEM) for mixed affinity binder (MAB, n = 5) and high affinity binder (HAB, n = 3) subjects and both groups combined (total, n = 8)

Brain region	Baseline V_T	Post-LPS V_T	%Δ V_T
Cerebellum			
MAB	2.57 ± 0.12	3.81 ± 0.34	47.8 ± 8.8
HAB	5.43 ± 0.31	7.40 ± 0.54	36.6 ± 13.1
Total	3.64 ± 0.56	5.15 ± 0.75	43.6 ± 7.1
Frontal			
MAB	2.58 ± 0.15	4.01 ± 0.38	54.3 ± 7.0
HAB	4.83 ± 0.37	6.87 ± 0.50	43.2 ± 13.1
Total	3.42 ± 0.47	5.08 ± 0.64	50.2 ± 5.7
Parietal			
MAB	2.62 ± 0.08	4.59 ± 0.46	74.6 ± 14.5
HAB	5.12 ± 0.41	7.38 ± 0.59	44.9 ± 10.7
Total	3.55 ± 0.52	5.63 ± 0.67	63.5 ± 10.8
Temporal			
MAB	2.39 ± 0.12	3.78 ± 0.37	57.3 ± 10.2
HAB	4.67 ± 0.30	6.58 ± 0.43	41.5 ± 11.2
Total	3.25 ± 0.46	4.83 ± 0.61	51.4 ± 7.5
Occipital			
MAB	2.92 ± 0.15	4.63 ± 0.55	56.5 ± 12.1
HAB	5.22 ± 0.37	7.00 ± 0.41	35.7 ± 11.2
Total	3.79 ± 0.48	5.52 ± 0.59	48.7 ± 9.0
Caudate			
MAB	1.90 ± 0.08	3.22 ± 0.35	67.6 ± 12.6
HAB	3.53 ± 0.24	4.89 ± 0.37	38.5 ± 3.7
Total	2.51 ± 0.33	3.85 ± 0.43	56.7 ± 9.3
Putamen			
MAB	2.16 ± 0.15	3.24 ± 0.25	50.8 ± 8.3
HAB	4.36 ± 0.34	6.09 ± 0.50	40.2 ± 9.9
Total	2.99 ± 0.45	4.31 ± 0.61	46.8 ± 6.3
Thalamus			
MAB	2.47 ± 0.16	3.21 ± 0.20	30.3 ± 4.8
HAB	5.45 ± 0.48	7.21 ± 0.61	33.3 ± 7.6
Total	3.59 ± 0.62	4.71 ± 0.82	31.4 ± 3.8
Hippocampus			
MAB	2.35 ± 0.19	3.19 ± 0.26	36.7 ± 7.7
HAB	4.79 ± 0.39	6.42 ± 0.47	36.3 ± 15.4
Total	3.26 ± 0.51	4.40 ± 0.67	36.6 ± 6.8
Amygdala			
MAB	2.47 ± 0.22	3.14 ± 0.23	28.7 ± 7.8
HAB	4.68 ± 0.34	6.55 ± 0.58	43.0 ± 22.6
Total	3.30 ± 0.47	4.42 ± 0.72	34.1 ± 9.1

LPS Administration Induces Sickness Symptoms and Related Behaviors. LPS is well known for its ability to produce sickness behaviors in preclinical (14, 38–41) and clinical (33, 36, 42) studies, and it is thought that these symptoms result from the effect on the brain of the increases in blood serum levels of cytokines. Subjects were asked to rate sickness symptoms (fatigue, headache, muscle pain, and shivering) on a scale from 0 (least) to 4 (most) before and at various time points after LPS administration (Fig. 2*B*). Self-reported sickness symptoms significantly increased from baseline, consistent with previous studies (Fig. 2*B*). Other symptoms known to be associated with LPS administration were measured on a visual analog scale (VAS) from 0 to 100 (Fig. 2*C*). The significant elevation in self-reported fatigue levels and significant reduction in social interest after LPS was consistent with previous findings (33, 36).

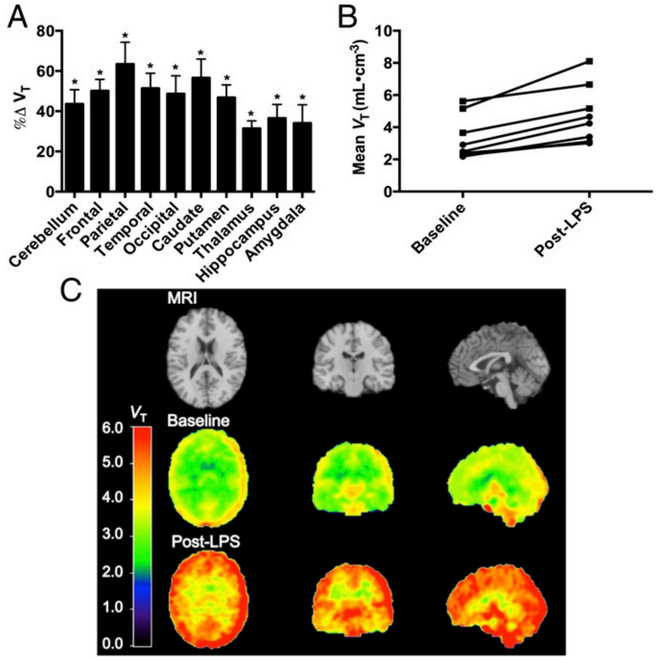

Fig. 1. LPS administration significantly increases [^{11}C]PBR28 binding (V_T) from baseline in healthy control subjects ($n = 8$) shown in *A*, regional percent increase in V_T averaged across subjects (error bars are SEM). (*B*) V_T for each subject averaged across regions examined in high-affinity (squares) and mixed-affinity binders (circles), and (*C*) average V_T images with the magnetic resonance image (MRI) shown for anatomical reference (*Top* row). Significance level was $*P < 0.01$ (linear mixed models) of the difference between baseline and post-LPS challenge scans.

Correlation of Binding Measures and Behavioral and Cytokine Data. In this small sample, significant correlations were not found between [^{11}C]PBR28 ΔV_T and changes in inflammatory cytokine or sickness symptoms from baseline levels.

Discussion

To our knowledge, we report for the first time in humans that a systemic LPS challenge elicits a robust and measurable neuroinflammatory response, in addition to the well-established effects of LPS on peripheral cytokine levels, sickness symptoms, and vital signs (14, 32, 33, 41). The pathway through which LPS activates the innate immune system is well established. LPS binds to toll-like receptor 4 on innate immune cells, leading to activation of these cells and the release of proinflammatory cytokines. The mechanism by which LPS exerts its effects on the brain (e.g., sickness symptoms, body temperature increase, and activation of microglia) are not completely known, but hypotheses include binding of LPS to toll-like receptor 4 on brain endothelium, transport of cytokines from the blood into the brain, and entry from the blood into the brain of activated immune cells (33).

Possibly due to the small cohort and intersubject variability in brain and peripheral and sickness measures in the current study, no correlations were found between [^{11}C]PBR28 ΔV_T and changes in inflammatory cytokine or sickness symptoms from baseline levels. The absence of correlations between the peripheral and central inflammatory response is consistent with other studies that had larger sample sizes. In a study where patients with major depressive episodes had higher TSPO V_T compared with healthy controls, no correlations were found between serum cytokines and brain TSPO binding, even after controlling for genotype and body mass index (27). Another study showed no correlations between cytokines in the serum and cerebrospinal fluid in patients before and after knee surgery, where cytokine levels were higher in the CNS than in the periphery after surgery (43). The authors surmise that although peripheral inflammation presumably induces the central inflammatory response, the CNS might regulate inflammation independently. Thus, lack of correlation between LPS-induced microglial activation and inflammatory cytokine levels may also reflect that the peripheral inflammatory markers are not a direct indicator of the brain changes, hence the importance of the [^{11}C]PBR28-LPS imaging paradigm.

The peripheral and behavioral effects of LPS are well established in rodent models and humans in studies of the immune mechanisms of CNS diseases. In the current study, systemic LPS markedly increased [^{11}C]PBR28 binding in humans. [^{11}C]PBR28 is a radioligand sensitive to TSPO levels expressed on activated microglia and is a putative biomarker for neuroinflammation. TSPO is also expressed in astrocytes; however, immunohistochemistry performed in a nonhuman primate brain after LPS administration confirmed that TSPO expression occurred mainly in activated microglia (32). To estimate the nonspecific binding contribution to [^{11}C]PBR28 V_T, a blocking study with TSPO agonist XBD173 in humans confirmed that [^{11}C]PBR28 V_T largely constitutes specific binding to TSPO (44). Thus, with the current imaging paradigm, the neuroimmune response to LPS can be quantitatively measured in vivo with [^{11}C]PBR28 and PET, in association with peripheral inflammation and sickness symptoms.

Results from the present study extend our previous findings using a similar paradigm in nonhuman primates. Specifically, in the current study, LPS administration (1.0 ng/kg, i.v.) led to increased [^{11}C]PBR28 binding levels by 46.3 ± 10.1% (mean ± SD, range 31.4–63.5%) at 3 h post-LPS, which was similar to the increases found in nonhuman primates (28.8 ± 15.7% and 61.8 ± 34.4%, at 1 h and 4 h post-LPS (0.1 mg/kg), respectively) (32). There are important species differences in the sensitivity to LPS. Some species, like humans and sheep, are very sensitive to LPS, whereas other species, such as mice and nonhuman primates are much more resistant. For instance, the LD_{50} dose of LPS in mice is 10^6 times greater than the typical doses used in humans (45). The dose used in our previous NHP study (0.1 mg/kg) is equivalent to a 4 ng/kg dose in humans in terms of blood levels of inflammatory cytokines (46). In both studies, the neuroinflammatory response was accompanied by an increase in blood levels of various inflammatory cytokines, including TNF-α, IL-6, IL-8, and IL-10. The physiological response was also similar between humans and nonhuman primates. Thus, we have successfully extended the main findings of the nonhuman primate study to human subjects and established that LPS administration in humans is associated with a marked and significant increase in activated microglia.

We expect that the increase in activated microglia measured with our paradigm is the "classically activated" microglia. Activated states of microglia can be of M1 type (classically activated) that are proinflammatory and neurodegenerative or M2 type ("alternatively activated") that are antiinflammatory and neuroprotective, with further classification as regulatory and wound healing (29, 47). However, it is important to note that this dichotomy is an oversimplification and that microglial activation ranges in a phenotypic spectrum between the two M1- and M2-type extremes (29, 48, 49). LPS has been routinely used in preclinical studies and is known to polarize microglia to an M1 phenotype, as characterized by brain mRNA expression of proinflammatory cytokines (e.g., TNF-α and IL-6) or immunophenotyping cell surface markers (e.g., MHC-II) (48). In the current study, a significant increase in TNF-α from baseline levels was observed 60 min post-LPS, peaking earlier than the other cytokines measured. TNF-α is a primary proinflammatory marker and plays an important role in the activation and recruitment of immune cells (50). Interestingly, antiinflammatory IL-10 levels also increased from baseline as a possible signaling mechanism to "switch off" M1 and "switch on" M2 microglia to regulate the neuroinflammatory process, as cytokines and sickness symptom levels appeared to be

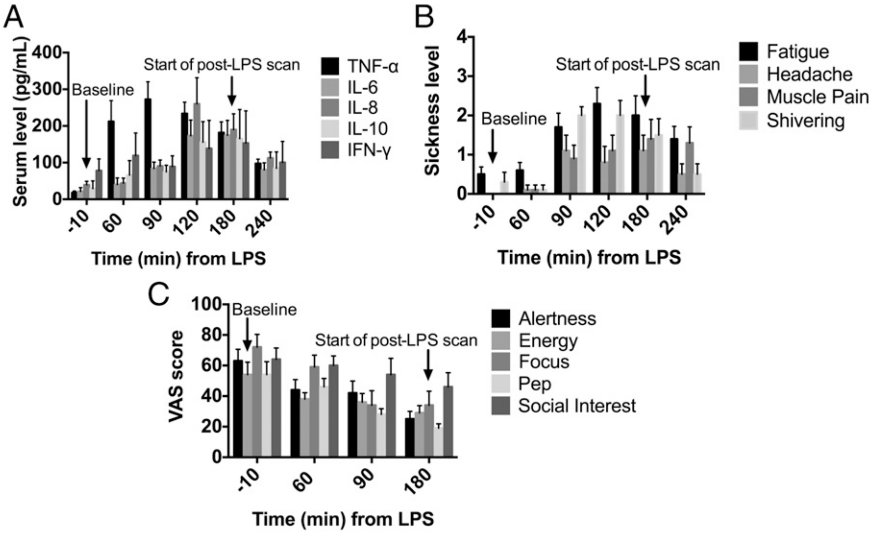

Fig. 2. LPS administration significantly increased (*A*) inflammatory cytokine serum levels, (*B*) sickness symptom levels, and (*C*) sickness symptoms measured on a visual analog scale (VAS) from baseline levels ($t = -10$ min). Times are relative to LPS administration at $t = 0$ min. LPS was administered 180 min before the start of the [^{11}C]PBR28 post-LPS scan. Data shown are the mean ($n = 8$ subjects) and error bars are SEM.

decreasing 1 h into the scan (240 min post-LPS). [^{11}C]PBR28 does not differentiate between M1- and M2-activated states; thus, an important development would be the ability to use PET imaging to measure M2-type activation of microglia in the brain. Because LPS is known to activate M1-type microglia, the [^{11}C]PBR28-LPS paradigm provides a useful tool for studying antiinflammatory drugs that reduce the neurodegenerative, M1-type microglia.

To date, the examination of immunomodulatory agents on microglial activation has been limited to preclinical and postmortem human studies (51–53). A potential application of the [^{11}C]PBR28-LPS model is to test medications designed to temper neuroinflammation, e.g., the neuroinflammation implicated in early onset (<65 y old) Alzheimer's disease (22). Alzheimer's disease is characterized by neurofibrillary tangles, beta-amyloid (Aβ) senile plaques, neuron loss, and cognitive/mood deficits. It has been shown in rodent models that initial aggregation of activated microglia around protofibrillar $A\beta_{42}$ plays a protective role and acts as a physical barrier to prevent further plaque expansion, whereas areas lacking microglia had protofibrillar "hotspots" with higher $A\beta_{42}$ affinity and greater axonal dystrophy (54). However, dysregulation of the M1 cycle, with the activation of the complement system and production of reactive oxygen species, inflammatory cytokines and chemokines, may lead to the progression of neurodegeneration in Alzheimer's disease where microglia eventually become senescent in late onset (55). An ideal antiinflammatory drug candidate would reduce M1-type microglial activation, target key peripheral immunomodulators that would promote M2-type neuroprotective/phagocytic microglia, and ameliorate cognitive symptoms. Most evidence suggests that inhibiting M1 and facilitating M2 microglia would be a beneficial mechanism to reduce neuroinflammation, but the roles of these two phenotypes in diseases are not completely understood. The [^{11}C]PBR28-LPS paradigm would be ideal for use as a biomarker of target modulation in phase 1 studies in healthy human subjects before the start of clinical trials in patients. For example, this imaging paradigm could provide insight into the mechanisms of known polarizing medications [e.g., minocycline (56) and TREM-2 agents (57)] and permit the assessment of novel antiinflammatory compounds to determine an optimal dose, based on the dose-dependent reductions in LPS-induced microglial activation. Due to the translational nature of this research paradigm, nonhuman primate or rodent models of Alzheimer's disease or Parkinson's disease would also be ideal to assess candidate antiinflammatory medications.

An important caveat to performing studies with [^{11}C]PBR28 is that the binding affinity of [^{11}C]PBR28 is dependent on the presence of a single nucleotide polymorphism rs6971 on the TSPO gene (34, 35). Thus, subjects must be genotyped before the PET scan to determine binding phenotypes, classified as HABs, MABs, or low-affinity binders (LABs); LABs were not included in the study due to negligible specific binding for [^{11}C]PBR28 (*Materials and Methods*). To date, the significance of the rs6971 polymorphism is undetermined (58). Knowledge of the binding phenotype is critical for studies comparing baseline TSPO levels between patients and healthy controls as previously demonstrated (35, 59). As expected in our healthy control cohort, baseline V_T values were 50% higher in HABs than MABs, but interestingly, the TSPO response to LPS (%Δ V_T) was independent of the subjects' binding affinity. LPS increased [^{11}C]PBR28 V_T from by 19–57% in HABs and 27–70% in MABs.

In conclusion, to our knowledge, this is the first study in humans to demonstrate the effects of LPS administration on microglial activation, measured with [^{11}C]PBR28 and PET brain imaging. As hypothesized, LPS significantly increased [^{11}C]PBR28 binding, peripheral inflammatory cytokine levels, and self-reported sickness symptoms. The [^{11}C]PBR28-LPS model is a valuable research paradigm that is broadly applicable to neuroinflammation-related diseases and can serve as an in vivo imaging marker of microglial activation to test neuroprotective and antiinflammatory drug candidates in humans.

Materials and Methods

Subjects. Eight healthy nonsmoker male subjects (24.9 ± 5.5 y old, 87.5 ± 12.3 kg) provided written informed consent and participated in the study. This study was approved by the Yale University School of Medicine Human Investigation Committee and the Radioactive Drug Research Committee. Participants were recruited by word of mouth, posters, and newspaper advertisements.

Eligibility was determined as follows: a medical examination including a physical examination, electrocardiogram, serum chemistries, thyroid, liver, and kidney function studies, HIV, syphilis, and hepatitis serologies, complete blood count, urinalysis, and urine toxicology screening. Subjects had no history of significant medical illness or major head trauma, did not meet criteria for any current or past psychiatric or substance-dependence diagnosis determined by the Structured Clinical Interview for Diagnostic and Statistical Manual of Mental Disorders (SCID) and clinical interview, had not used psychotropic medications in at least the prior year, and drank fewer than seven alcohol drinks per week. Subjects were excluded if they had an infection or vaccination in the last month or regularly used nonsteroidal antiinflammatory drugs. Subjects had not used nonsteroidal antiinflammatory drugs in the last month and were instructed to abstain from alcohol 48 h before the day of the scan. Before the scan, subjects were genotyped for the rs6971 polymorphism on the TSPO gene to exclude nonbinders of [^{11}C]PBR28 as previously described, with minor changes to include the use of 50 ng of genomic DNA in the PCR (24, 34). Control plasmids (constructed in house) encoded for C/C (HAB) or T/T (LAB) and a 1:1 mixture of each to serve as a control for the C/T heterozygote (MAB).

Each subject participated in two [^{11}C]PBR28 PET scans on the same day, one baseline scan and a second scan starting at 180 min after LPS administration. The order of scans was not randomized across subjects; the baseline scan was always performed before the LPS challenge scan to avoid the possibility of carry-over microglial activation from the LPS scan to the baseline scan. We have recently demonstrated excellent test–retest variability of [^{11}C]PBR28 V_T between 7% and 9%, with scans performed approximately 1 wk apart (26). Because test–retest variability for PET scans performed on the same day is typically less variable compared with scans performed on separate days, it is unlikely that a test–retest change in V_T from a morning to an afternoon scan would significantly affect LPS-induced changes. On a separate day, each subject had one magnetic resonance imaging (MRI) scan, to provide anatomical information for analysis of the PET data.

LPS Administration and Measures. LPS (NIH Clinical Center Reference Endotoxin *E. coli* serotype O:113) was administered at a dose of 1.0 ng/kg, i.v. Vital signs (temperature, blood pressure, and heart rate) were recorded before and at 60, 90, 120, 180, 240 min, and 300 min (incomplete subject data) after LPS administration. Blood samples were drawn to measure inflammatory cytokine levels of TNF-α, IL-6, IL-8, IL-10, and IFN-γ relative to LPS administration ($t = 0$ min) at -10 (baseline), 60, 90, 120, 180 {start of [^{11}C]PBR28 scan 2}, and 240 min. Sickness symptoms (fatigue, headache, muscle pain, and shivering) were assessed from a scale from 0 (least) to 4 (most) relative to LPS administration ($t = 0$ min) at −10, 60, 90, 120, 180, and 240 min. A VAS of 0 (least) to 100 (most) was used to evaluate symptoms such as alertness, energy, focus, pep, and social interest relative to LPS administration at −10, 60, 90, and 180 min.

[^{11}C]PBR28 PET Acquisition and Image Reconstruction. [^{11}C]PBR28 was synthesized as previously described (24). The specific activity at the end of synthesis (mean ± SD) was 569.0 ± 326.7 MBq/nmol (15.4 ± 8.8 mCi/nmol, $n =$ 16) and the average radiochemical and chemical purity was >91% and >99%, respectively. PET scans were performed in the High Resolution Research Tomograph (HRRT) (Siemens) with a spatial resolution, full width at half maximum of 2–3 mm. An optical motion-tracking tool (Vicra, NDI Systems) was attached to the subject's head with a Lycra swim cap. Before each radiotracer administration, a 6-min transmission scan was acquired, which was used for attenuation correction of the PET emission data. [^{11}C]PBR28 was injected i.v. as a bolus over 1 min by a computer-controlled pump (Harvard Apparatus), and emission data were collected for 120 min. Dynamic list-mode scan data were reconstructed into 33 frames (6×30 s, 3×1 min, 2×2 min, and 22×5 min) with all corrections (i.e., attenuation, normalization, randoms, scatter, deadtime, and motion) using the ordered-subset expectation maximization (OSEM)-based MOLAR algorithm (60). The final reconstructed image resolution was ∼3 mm.

Arterial Input Function and Plasma-Free Fraction Measurement. The metabolite-corrected arterial input function was collected for all scans and used for radiotracer kinetic modeling to estimate [^{11}C]PBR28 binding as previously described (24). Briefly, arterial blood samples were taken immediately before the [^{11}C]PBR28 injection and during the scan to measure the time course of radioactivity in the plasma and to determine the [^{11}C]PBR28 parent fraction curve (ratio of parent radioactivity to total radioactivity). The metabolite-corrected arterial input function was calculated as the product of the plasma time curve and the parent fraction curve.

Plasma free fraction (fp), or the portion of [^{11}C]PBR28 unbound to plasma protein, was determined for all scans using an ultrafiltration-based method as previously described (24).

Image Processing and Analysis. Regions of interest (ROIs) were mapped from Montreal Neurological Institute (MNI) template space to PET space to compute tissue time-activity curves (TACs), which represent the time course of mean radioactivity [(Bq/mL), corrected for decay] in the ROI. The following ROIs were assessed: cerebellum, frontal, parietal, temporal, occipital, caudate, putamen, thalamus, hippocampus, and amygdala. TACs were fitted to a two-tissue compartmental (2TC) model (61), using the metabolite-corrected arterial plasma activity curve as input function to estimate the volume of distribution (V_T, mL/cm^3) in each ROI. V_T is the equilibrium tissue to plasma activity ratio used to quantify [^{11}C]PBR28 binding (62). The change in V_T (%ΔV_T) across brain regions pre- and post-LPS was computed as $\%\Delta V_T = [V_T(\text{post})/V_T(\text{pre}) - 1] \times 100$. For visualization of activated microglia pre- and post-LPS, parametric images of V_T were generated using the LEGA method (63), with the starting time of the fit (t*) fixed at 30 min, and with basis functions computed with parameter γ (i.e., the y-intercept of the Logan plot) values in the range between −200 min and −1 min. Before applying the model, the dynamic images were smoothed with a Gaussian filter with a full width at half maximum of 5 voxels (∼6 mm).

Statistical Analysis. Statistical analysis was performed with two-tailed, paired t tests with $P < 0.05$ to examine differences in [^{11}C]PBR28 scan parameters between baseline and LPS challenge and differences in vital signs (mean ± SD) between baseline ($t = -10$ min) and post-LPS ($t = 180$ min).

Across subjects, [^{11}C]PBR28 V_T, cytokine levels, and sickness symptom data are reported as mean ± SEM. The observed percent change from baseline in V_T (%ΔV_T) was analyzed using a linear mixed model with region modeled as a within-subjects factor. Least-square means and SEs were estimated from the model and tested against the null of no change. A similar model was used to model changes in cytokines and sickness variables with time, in lieu of region, as the within-subjects variable. In the above models, group (HAB and MAB) was considered as a between-subjects factor, but dropped for parsimony if not significant. Correlation analysis was used to test for associations between binding measures and behavioral and cytokine outcomes.

ACKNOWLEDGMENTS. The authors thank Erin McGovern, Evgenia Perkins, Lesley Devine, the staff at the Yale PET Center, and Dr. Ming-Kai Chen. Research support was provided by UCB Pharma.

1. Kostic M, Stojanovic I, Marjanovic G, Zivkovic N, Cvetanovic A (2015) Deleterious versus protective autoimmunity in multiple sclerosis. *Cell Immunol* 296(2):122–132.
2. Cameron B, Landreth GE (2010) Inflammation, microglia, and Alzheimer's disease. *Neurobiol Dis* 37(3):503–509.
3. Hurley LL, Tizabi Y (2013) Neuroinflammation, neurodegeneration, and depression. *Neurotox Res* 23(2):131–144.
4. Kelley KW, Dantzer R (2011) Alcoholism and inflammation: Neuroimmunology of behavioral and mood disorders. *Brain Behav Immun* 25(Suppl 1):S13–S20.
5. Streit WJ, Mrak RE, Griffin WS (2004) Microglia and neuroinflammation: A pathological perspective. *J Neuroinflammation* 1(1):14.
6. Heneka MT, et al. (2015) Neuroinflammation in Alzheimer's disease. *Lancet Neurol* 14(4):388–405.
7. Marchi N, Granata T, Janigro D (2014) Inflammatory pathways of seizure disorders. *Trends Neurosci* 37(2):55–65.
8. Moehle MS, West AB (2015) M1 and M2 immune activation in Parkinson's Disease: Foe and ally? *Neuroscience* 302:59–73.
9. Aloisi F (2001) Immune function of microglia. *Glia* 36(2):165–179.
10. Carson MJ, et al. (2007) A rose by any other name? The potential consequences of microglial heterogeneity during CNS health and disease. *Neurotherapeutics* 4(4):571–579.
11. Kettenmann H, Kirchhoff F, Verkhratsky A (2013) Microglia: New roles for the synaptic stripper. *Neuron* 77(1):10–18.
12. Dheen ST, Kaur C, Ling EA (2007) Microglial activation and its implications in the brain diseases. *Curr Med Chem* 14(11):1189–1197.
13. Zhao YN, et al. (2013) Activated microglia are implicated in cognitive deficits, neuronal death, and successful recovery following intermittent ethanol exposure. *Behav Brain Res* 236(1):270–282.
14. Dantzer R, O'Connor JC, Freund GG, Johnson RW, Kelley KW (2008) From inflammation to sickness and depression: When the immune system subjugates the brain. *Nat Rev Neurosci* 9(1):46–56.
15. Yirmiya R, Goshen I (2011) Immune modulation of learning, memory, neural plasticity and neurogenesis. *Brain Behav Immun* 25(2):181–213.
16. Papadopoulos V, et al. (2006) Translocator protein (18 kDa): New nomenclature for the peripheral-type benzodiazepine receptor based on its structure and molecular function. *Trends Pharmacol Sci* 27(8):402–409.
17. Doorduin J, de Vries EF, Dierckx RA, Klein HC (2008) PET imaging of the peripheral benzodiazepine receptor: Monitoring disease progression and therapy response in neurodegenerative disorders. *Curr Pharm Des* 14(31):3297–3315.
18. Fujita M, et al. (2008) Kinetic analysis in healthy humans of a novel positron emission tomography radioligand to image the peripheral benzodiazepine receptor, a potential biomarker for inflammation. *Neuroimage* 40(1):43–52.
19. Liu GJ, et al. (2014) The 18 kDa translocator protein, microglia and neuroinflammation. *Brain Pathol* 24(6):631–653.

20. Venneti S, Lopresti BJ, Wiley CA (2006) The peripheral benzodiazepine receptor (Translocator protein 18 kDa) in microglia: From pathology to imaging. *Prog Neurobiol* 80(6):308–322.
21. Bae KR, Shim HJ, Balu D, Kim SR, Yu SW (2014) Translocator protein 18 kDa negatively regulates inflammation in microglia. *J Neuroimmune Pharmacol* 9(3):424–437.
22. Kreisl WC, et al. (2013) In vivo radioligand binding to translocator protein correlates with severity of Alzheimer's disease. *Brain* 136(Pt 7):2228–2238.
23. Colasanti A, et al. (2014) In vivo assessment of brain white matter inflammation in multiple sclerosis with (18)F-PBR111 PET. *J Nucl Med* 55(7):1112–1118.
24. Hannestad J, et al. (2013) The neuroinflammation marker translocator protein is not elevated in individuals with mild-to-moderate depression: A [^{11}C]PBR28 PET study. *Brain Behav Immun* 33:131–138.
25. Narendran R, et al. (2014) Cocaine abuse in humans is not associated with increased microglial activation: An 18-kDa translocator protein positron emission tomography imaging study with [11C]PBR28. *J Neurosci* 34(30):9945–9950.
26. Park E, et al. (2015) (11)C-PBR28 imaging in multiple sclerosis patients and healthy controls: Test-retest reproducibility and focal visualization of active white matter areas. *Eur J Nucl Med Mol Imaging* 42(7):1081–1092.
27. Setiawan E, et al. (2015) Role of translocator protein density, a marker of neuroinflammation, in the brain during major depressive episodes. *JAMA Psychiatry* 72(3): 268–275.
28. Tufekci KU, Genc S, Genc K (2011) The endotoxin-induced neuroinflammation model of Parkinson's disease. *Parkinsons Dis* 2011:487450.
29. Mosser DM, Edwards JP (2008) Exploring the full spectrum of macrophage activation. *Nat Rev Immunol* 8(12):958–969.
30. Nakagawa Y, Chiba K (2014) Role of microglial m1/m2 polarization in relapse and remission of psychiatric disorders and diseases. *Pharmaceuticals (Basel)* 7(12):1028–1048.
31. Cunningham C (2013) Microglia and neurodegeneration: The role of systemic inflammation. *Glia* 61(1):71–90.
32. Hannestad J, et al. (2012) Endotoxin-induced systemic inflammation activates microglia: [^{11}C]PBR28 positron emission tomography in nonhuman primates. *Neuroimage* 63(1): 232–239.
33. Schedlowski M, Engler H, Grigoleit JS (2014) Endotoxin-induced experimental systemic inflammation in humans: A model to disentangle immune-to-brain communication. *Brain Behav Immun* 35:1–8.
34. Owen DR, et al. (2012) An 18-kDa translocator protein (TSPO) polymorphism explains differences in binding affinity of the PET radioligand PBR28. *J Cereb Blood Flow Metab* 32(1):1–5.
35. Kreisl WC, et al. (2013) A genetic polymorphism for translocator protein 18 kDa affects both in vitro and in vivo radioligand binding in human brain to this putative biomarker of neuroinflammation. *J Cereb Blood Flow Metab* 33(1):53–58.
36. Hannestad J, et al. (2012) Glucose metabolism in the insula and cingulate is affected by systemic inflammation in humans. *J Nucl Med* 53(4):601–607.
37. Biswas SK, Lopez-Collazo E (2009) Endotoxin tolerance: New mechanisms, molecules and clinical significance. *Trends Immunol* 30(10):475–487.
38. Camara ML, et al. (2015) Effects of centrally administered etanercept on behavior, microglia, and astrocytes in mice following a peripheral immune challenge. *Neuropsychopharmacology* 40(2):502–512.
39. Delpech JC, et al. (2015) Transgenic increase in n-3/n-6 fatty acid ratio protects against cognitive deficits induced by an immune challenge through decrease of neuroinflammation. *Neuropsychopharmacology* 40(3):525–536.
40. Zheng X, et al. (2014) Peripheral immunomodulation with ginsenoside Rg1 ameliorates neuroinflammation-induced behavioral deficits in rats. *Neuroscience* 256:210–222.
41. Biesmans S, et al. (2013) Systemic immune activation leads to neuroinflammation and sickness behavior in mice. *Mediators Inflamm* 2013:271359.
42. Hannestad J, DellaGioia N, Ortiz N, Pittman B, Bhagwagar Z (2011) Citalopram reduces endotoxin-induced fatigue. *Brain Behav Immun* 25(2):256–259.
43. Bromander S, et al. (2012) Changes in serum and cerebrospinal fluid cytokines in response to non-neurological surgery: An observational study. *J Neuroinflammation* 9:242.
44. Owen DR, et al. (2014) Determination of [(11)C]PBR28 binding potential in vivo: A first human TSPO blocking study. *J Cereb Blood Flow Metab* 34(6):989–994.
45. Fink MP (2014) Animal models of sepsis. *Virulence* 5(1):143–153.
46. Haudek SB, et al. (2003) Lipopolysaccharide dose response in baboons. *Shock* 20(5): 431–436.
47. Orihuela R, McPherson CA, Harry GJ (2015) Microglial M1/M2 polarization and metabolic states. *Br J Pharmacol*, in press.
48. Boche D, Perry VH, Nicoll JA (2013) Review: Activation patterns of microglia and their identification in the human brain. *Neuropathol Appl Neurobiol* 39(1):3–18.
49. Kreutzberg GW (1996) Microglia: A sensor for pathological events in the CNS. *Trends Neurosci* 19(8):312–318.
50. Fischer R, Maier O. (2015) Interrelation of oxidative stress and inflammation in neurodegenerative disease: Role of TNF. *Oxid Med Cell Longev* 2015:610813.
51. Zotova E, et al. (2011) Microglial alterations in human Alzheimer's disease following Aβ42 immunization. *Neuropathol Appl Neurobiol* 37(5):513–524.
52. Giunti D, Parodi B, Cordano C, Uccelli A, Kerlero de Rosbo N (2014) Can we switch microglia's phenotype to foster neuroprotection? Focus on multiple sclerosis. *Immunology* 141(3):328–339.
53. McGeer PL, McGeer EG (2015) Targeting microglia for the treatment of Alzheimer's disease. *Expert Opin Ther Targets* 19(4):497–506.
54. Condello C, Yuan P, Schain A, Grutzendler J (2015) Microglia constitute a barrier that prevents neurotoxic protofibrillar Aβ42 hotspots around plaques. *Nat Commun* 6: 6176.
55. Li Y, Tan MS, Jiang T, Tan L (2014) Microglia in Alzheimer's disease. *Biomed Res Int* 2014:437483.
56. Garrido-Mesa N, Zarzuelo A, Gálvez J (2013) Minocycline: Far beyond an antibiotic. *Br J Pharmacol* 169(2):337–352.
57. Yaghmoor F, et al. (2014) The role of TREM2 in Alzheimer's disease and other neurological disorders. *J Alzheimers Dis Parkinsonism* 4(5):160.
58. Zanotti-Fregonara P, et al. (2014) Synthesis and evaluation of translocator 18 kDa protein (TSPO) positron emission tomography (PET) radioligands with low binding sensitivity to human single nucleotide polymorphism rs6971. *ACS Chem Neurosci* 5(10):963–971.
59. Fan Z, et al. (2015) Can studies of neuroinflammation in a TSPO genetic subgroup (HAB or MAB) be applied to the entire AD cohort? *J Nucl Med* 56(5):707–713.
60. Carson REBW, Liow J-S, Adler S, Johnson CA (2003) Design of a motion-compensation OSEM list-mode algorithm for resolution-recovery reconstruction of the HRRT. *IEEE Nuclear Science Symposium and Medical Imaging Conference* 5:3281–3285.
61. Gunn RN, Gunn SR, Cunningham VJ (2001) Positron emission tomography compartmental models. *J Cereb Blood Flow Metab* 21(6):635–652.
62. Innis RB, et al. (2007) Consensus nomenclature for in vivo imaging of reversibly binding radioligands. *J Cereb Blood Flow Metab* 27(9):1533–1539.
63. Ogden RT (2003) Estimation of kinetic parameters in graphical analysis of PET imaging data. *Stat Med* 22(22):3557–3568.

IMMUNOLOGY AND INFLAMMATION